JMEPEG (2005) 14:773-777
DOI: 10.1361/105994905X75592

1059-9495/$19.00

High-Cycle Fatigue Crack Initiation and Growth in TIMETAL LCB

Basak Yazgan Kokuoz, Yoji Kosaka, and H.J. Rack

(Submitted August 24, 2005)

This investigation has examined the influence of grain boundary α contiguity on the high-cycle fatigue behavior of aged TIMETAL LCB, with the fatigue performance being evaluated under tension-tension loading conditions at $R = 0.1$ in laboratory air and 25 Hz. Fractographic analysis indicated that fatigue initiation, independent of processing history, involved subsurface crack formation. Serial section studies also indicated that crack initiation occurred at the interface between the triple-point α and the aged β matrix. Further back-scattered electron microscopy examination of the aged microstructures indicates that the observed differences in high-cycle fatigue behavior can be understood by considering the effect of processing history on the connectivity of grain boundary α, with decreased connectivity being associated with enhanced fatigue performance.

Keywords contiguity, high cycle fatigue, metastable β titanium

1. Introduction

Metastable β titanium alloys are receiving ever-increasing attention for possible incorporation into automotive suspension systems. Their strength-to-density ratio, high toughness, and low modulus make them attractive candidates for these applications (Ref 1). However, their low high-cycle fatigue performance, when compared with α + β titanium alloys at equivalent yield strength (Ref 2, 3), has tended to limit their utility, although some recent progress has been made in this regard (Ref 4, 5).

Normally, the high-cycle fatigue performance of metallic materials is thought to be controlled by crack initiation, with the crack propagation stage playing a relatively minor role. Past experience suggests that the former, in aged metastable β titanium alloys, can be associated with crack initiation at grain boundary α (Ref 6, 7). These observations indicate that it should be possible to enhance the high-cycle fatigue performance of aged metastable β titanium alloys through the control of the thermomechanical history of the alloy. For example, various combinations of thermomechanical processing conditions have been shown to increase fatigue the crack initiation resistance of metastable β titanium alloys (Ref 8, 9).

In the current study, the effects of two different processing conditions on the high-cycle fatigue performance of TIMETAL LCB were investigated. These will be referred to as A and B processing hereafter. Particular attention has been given to quantifying the microstructures produced by these thermomechanical processing pathways, with a preliminary model being proposed linking the contiguity of grain boundary α and high-cycle fatigue crack initiation.

This paper was presented at the Beta Titanium Alloys of the 00's Symposium sponsored by the Titanium Committee of TMS, held during the 2005 TMS Annual Meeting & Exhibition, February 13-16, 2005 in San Francisco, CA.

Basak Yazgan Kokuoz and **H.J. Rack,** Clemson University, School of Materials Science & Engineering, Clemson, SC 29634-0971; **Yoji Kosaka,** TIMET, HTL, P.O. Box 2128, Henderson, NV 89015. Contact e-mail: rackh@clemson.edu.

2. Experimental Procedures

The high-cycle fatigue performance of A- and B-processed TIMETAL LCB was examined in this study. This performance was quantified by axial fatigue tests under tension-tension loading conditions at $R = 0.1$ in laboratory air at 25 Hz. The specimens had a 37.5 mm reduced section and a 4.5 mm reduced diameter. Following machining, the samples were polished to a 600-grit SiC finish, with the fatigue experiments being terminated either by failure or after 10^7 cycles. The chemical composition (in weight percent) of the A- and B-processed samples are shown in Table 1.

Microstructure examination of the A- and B-processed samples emphasized back-scattered electron microscopy (BSEI). The specimens examined were mechanically polished using standard procedures, with final polishing being performed with a colloidal silica solution. Quantitative image analysis (Image Processing Tool Kit, Version 5, Reindeer Graphics, Inc., Asheville, NC) was used to establish the prior β grain size together with the volume fraction and extent of contiguity of the grain boundary α phase. The results presented are an average of twelve 24×24 μm^2 areas at a magnification of 2500×. Grain size determination used the mean intercept method, the grain size being determined from the number of grain boundaries intersecting a unit length of randomly

Table 1 Chemical compositions of A and B processed samples

Samples	Al	Mo	Fe	Si	C	O	N
A processed	1.49	6.84	4.20	0.05	0.02	0.14	0.004
B processed	1.46	6.82	4.0	0.07	0.01	0.15	0.004

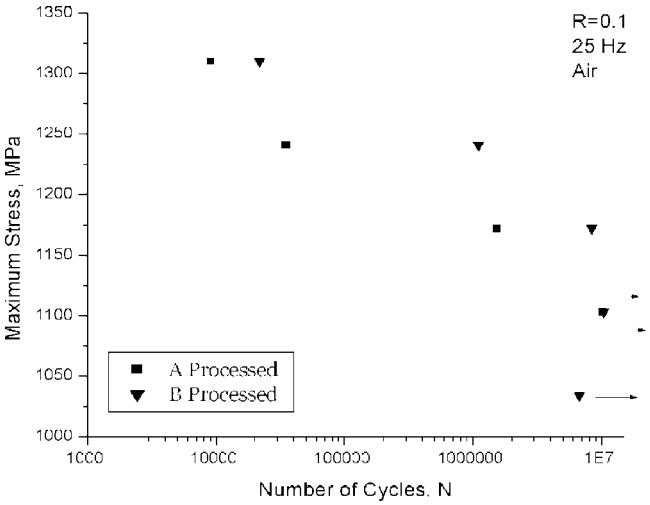

Fig. 1 Constant stress fatigue lifetimes for A- and B-processed TIMETAL LCB. $R = 0.1$ in air at 25 Hz

Table 2 Room temperature tensile properties of TIMETAL LCB

Samples	$\sigma_{0.2}$, MPa	UTS, MPa	El, %	RA, %
A processed	1376	1414	12.09	43.1
B processed	1365	1409	11.07	39.0

Note: UTS, ultimate tensile strength; El, elongation; RA, reduction in area

distributed test lines. Volume fraction measurements used point counting, with a point grid consisting of 200 randomly distributed points being used for this purpose. The number of points that fall within the grain boundary α phase was automatically counted, and the areal (volume) fraction was estimated from the number fraction of these points.

Three types of interfaces are also identified for contiguity measurements. These were the interface between continuous grain boundary α/triple-point α, $(P_L)_{\alpha(CGB)/\alpha(TP_1)}$, triple-point α interfaces that are bounded by a noncontinuous α, $(P_L)_{\alpha(TP_2)}$, and triple-point α that is not bounded by any grain boundary α, $(P_L)_{\alpha(TP_3)}$. The number of each type of interface intersecting with randomly distributed test lines was counted to establish the total fraction of the surface area of the continuous grain boundary α/triple-point interfaces.

Nano-indentation measurements within the grain boundary α phase and within the aged β matrix were also performed, the results reported herein represent the average of the seven indentations performed under a 300 μN peak load. Finally, the fracture surfaces of selected samples were examined by secondary imaging with scanning electron microscopy (SEM) using a voltage of 20 keV, at a working distance of 15 mm. Failed fatigue specimen sections were also prepared normal to the fatigue axis to allow the definition of possible fatigue crack initiation sites, these samples being mechanically polished prior to examination by BSEI.

3. Experimental Results and Discussion

The room temperature tensile properties of A- and B-processed samples are given in Table 2. These results indicate

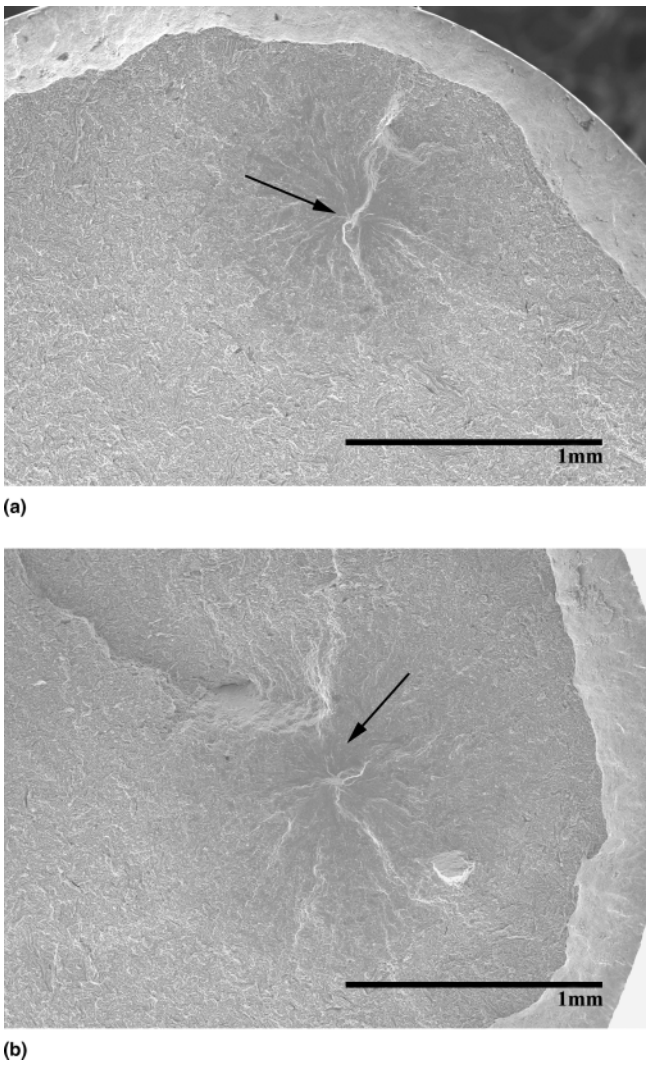

Fig. 2 Fatigue fracture surfaces of (a) an A-processed sample and (b) a B-processed sample

that the processing route had little effect on the properties. In contrast, the high cycle fatigue results shown in Fig. 1 indicate that B processing results in a consistently higher fatigue performance.

Figure 2 shows typical low-magnification, secondary SEM micrographs of the fracture surfaces. The black arrows on the figure indicate the crack-initiation sites; all fatigue failures, independent of processing history, were initiated at the specimen subsurface. This indicates that under the present loading conditions fatigue crack initiation is related to a microstructure phenomenon rather than to environmental effects. Figure 3 illustrates the resultant microstructures that were produced by the processing conditions considered in the present investigation. Quantitative image analysis results (Table 3) show that processing condition had little effect on the volume fraction of α and the grain size of the aged β matrix.

Nano-indentation measurements also show that, prior to fatigue loading, the grain boundary α phase is softer than the aged β matrix (Table 4). Similar measurements after fatigue suggest, however, that preferential deformation and damage accumulation has occurred within grain boundary α.

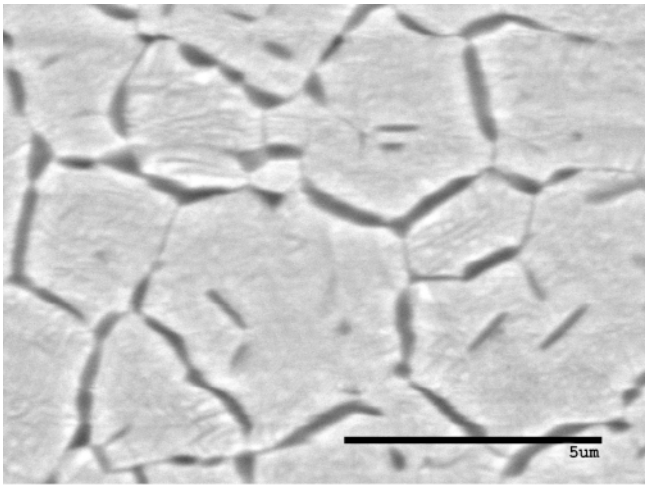

(a)

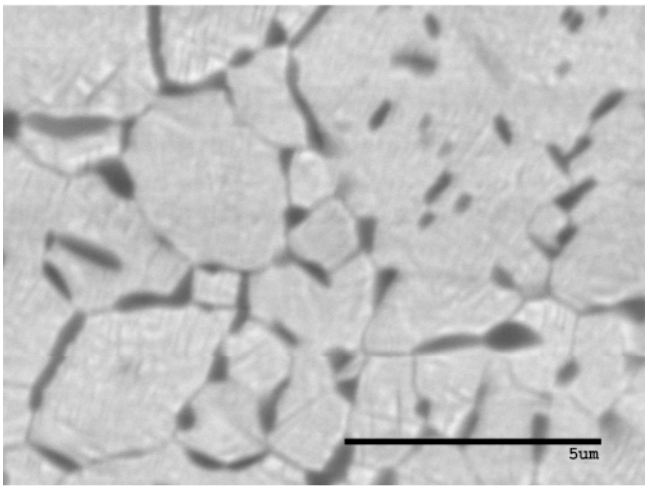

(b)

Fig. 3 Representative microstructures of (a) an A-processed sample and (b) a B-processed sample

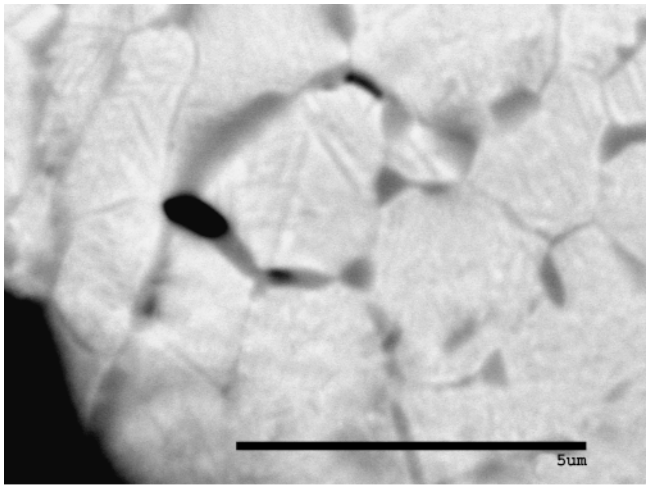

(a)

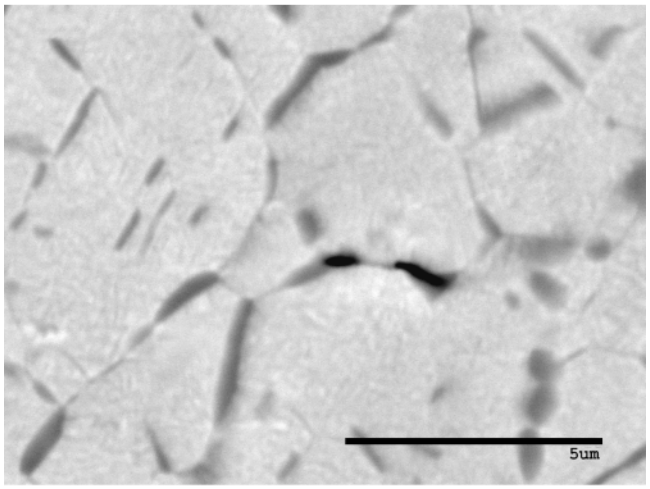

(b)

Fig. 4 Evidence of crack initiation at the α-β interface in (a) an A-processed sample and (b) a B-processed sample

BSEI examination of the sectioned samples also showed that fatigue crack initiation was associated with triple points (Fig. 4). These observations suggest that damage accumulation within grain boundary α and fatigue crack initiation are related. The critical stress for fatigue crack initiation, τ_c, may be estimated from (Ref 10):

$$\tau_c \propto \left(\frac{2G\gamma_s}{nb}\right)^{1/2} \quad \text{(Eq 1)}$$

where G is the shear modulus, γ is the surface energy, b is the Burger's vector, and n is the number of dislocations within a pile up, and where the stress intensification at the head of a dislocation array, τ_p, is given by:

$$\tau_p = n\tau \quad \text{(Eq 2)}$$

where τ is the applied shear stress and n is as defined above.

Additionally, the number of dislocations within the pile up can be taken to be proportional to the operative slip length, L:

$$n \propto L\tau \quad \text{(Eq 3)}$$

Combining Eq 2 through 3 gives:

$$\tau_c \propto L^{-1/2} \quad \text{(Eq 4)}$$

indicating that the resistance of the material to fatigue crack initiation should decrease with the square root of the operative slip length.

The operative slip length is often assumed to be proportional to the grain size, D:

$$L \propto D \quad \text{(Eq 5)}$$

In the present investigation, the operative slip length can be associated with the grain boundary α length. If the grain boundary α is continuous, the slip length may be correlated to the grain boundary length, L_{GB}:

$$L_{GB} \propto D \quad \text{(Eq 6)}$$

Then:

$$L \propto L_{GB} \quad \text{(Eq 7)}$$

Rewriting Eq 2 gives:

$$\tau_c \propto (L_{GB})^{1/2} \quad \text{(Eq 8)}$$

Table 3 Quantitative image analysis results of A and B processed TIMETAL LCB

Samples	Volume fraction	Grain size, μm
A processed	0.144	3.24
B processed	0.143	3.14

Table 4 Nanoindentation results performed on A and B processed specimens

Samples	Undeformed aged β matrix hardness, GPa	Undeformed grain boundary α hardness, GPa	Deformed grain aged β matrix hardness, GPa	Deformed grain boundary α hardness, GPa
A processed	3.24	2.48	0.32	6.65
B processed	3.62	2.54	1.05	5.62

Therefore, τ_c can be taken to be inversely proportional to the square root of the length of the continuous grain boundary α.

This relationship assumes that all triple-point α particles are bounded by continuous grain boundary α. However, three types of triple points were identified (Fig. 5). These are triple-point α bounded by a continuous grain boundary α, TP_1; triple-point α bounded by noncontinuous α, TP_2; and triple points that are not bounded by any grain boundary α, TP_3. If different fatigue crack initiation resistances are assumed for each, then the high cycle fatigue performance should depend upon the contiguity of continuous α at the triple points (Ref 11). Indeed, if this were not the case, the fatigue performance of the two processing conditions considered herein, due to their similar prior β grain size and volume fraction of α, should have resulted in similar fatigue properties.

The contiguity of continuous α at the triple points, $C_{\alpha(CGB)}$, can be defined as the frequency of finding a triple-point α bounded by a continuous grain boundary α. This may be determined by considering the total fraction of the surface area of continuous grain boundary α/triple point interfaces:

$$C_{\alpha(CGB)} = \frac{S_{V_{\alpha(CGB)/\alpha(TP_1)}}}{S_{V_{total}}} = \frac{(P_L)_{\alpha(CGB)/\alpha(TP_1)}}{(P_L)_{\alpha(CGB)/\alpha(TP_1)} + (P_L)_{\alpha(NC)/\alpha(TP_2)} + (P_L)_{\beta/\alpha(TP_3)}} \quad \text{(Eq 9)}$$

where $(P_L)_{\alpha(CGB)/\alpha(TP_1)}$, $(P_L)_{\alpha(NC)/\alpha(TP_2)}$, and $(P_L)_{\alpha(TP_3)}$ are the number of continuous grain boundary α/triple-point α, the triple-point α/noncontinuous α, and the triple-point α/aged β matrix interfaces intersecting with a unit test line. The mean contiguity ratios of A- and B-processed alloys are 0.56 ± 0.07 and 0.44 ± 0.01, respectively. These results indicate that the degree of contact between the continuous grain boundary α and the triple-point α particles controls fatigue crack initiation. Higher degrees of contiguity (i.e., contact) favor early fatigue crack initiation.

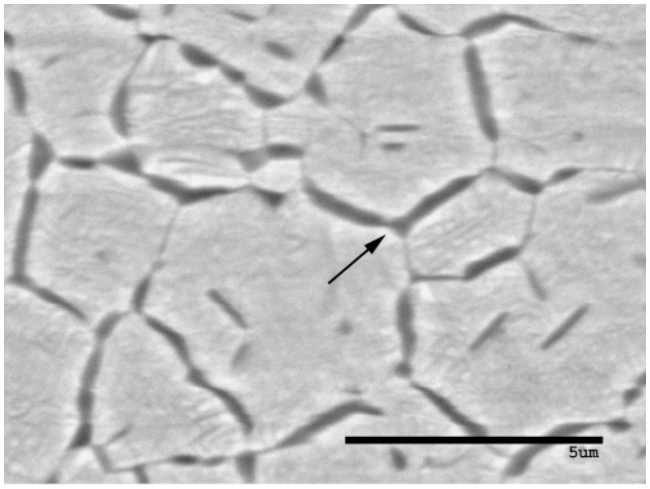

(a)

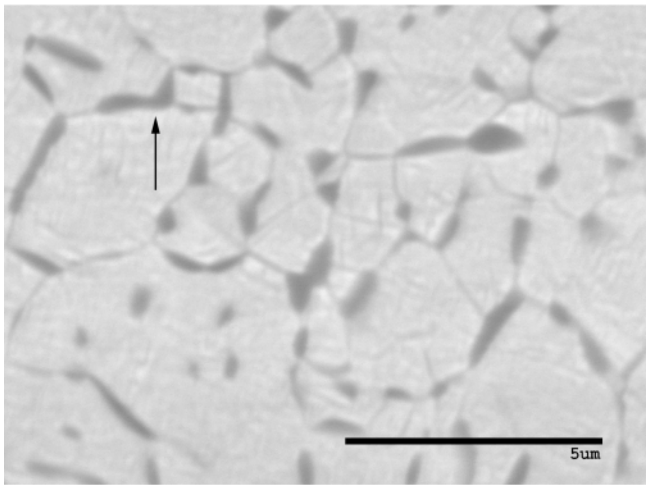

(b)

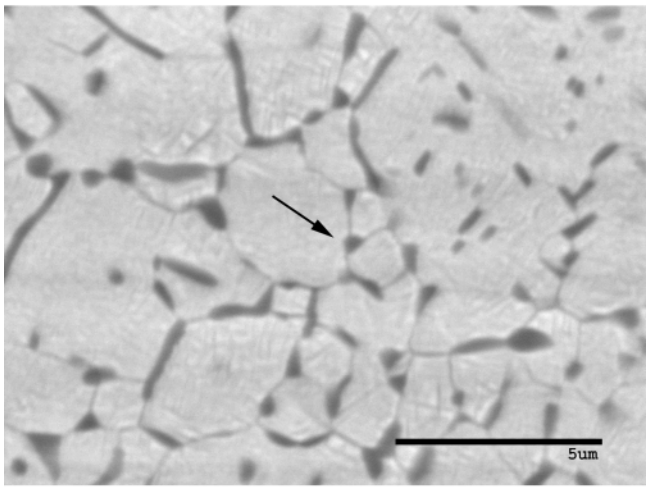

(c)

Fig. 5 Different types of triple points within the microstructure: (a) Triple-point α bounded by a continuous grain boundary α, TP_1; (b) Triple-point α bounded by noncontinuous α, TP_2; (c) Triple points that are not bounded by any grain boundary α, TP_3

4. Conclusions

This investigation has shown that under equivalent tensile properties, α volume fraction, and prior β grain size, the high-cycle fatigue behavior of TIMETAL LCB is controlled by the contiguity of the grain boundary α phase; with a higher contiguity ratio being associated with a decreased crack initiation resistance.

Acknowledgments

The authors would like to acknowledge TIMET for their financial support, Dr. John Russ for his valuable assistance with the image analysis procedures, and Mr. Baris Kokuoz for his help during nano-indentation measurements.

References

1. P.J. Bania, Beta Titanium Alloys and Their Role in the Titanium Industry, *Beta Titanium Alloys of the 1990s,* 1st ed., D. Eylon, R.R. Boyer, and D.A. Koss, Ed., The Materials Society, 1993, p 211-226
2. L. Wagner and J.K. Gregory, Fatigue and Fracture Properties of Titanium Alloys, *ASM Handbook,* Vol 19, ASM International, p 829-853
3. J.C. Fanning, Fatigue Data for TIMETAL 15-3, *Beta Titanium Alloys of the 1990s,* 1st ed., D. Eylon, R.R. Boyer, and D.A. Koss, Ed., The Materials Society, 1993, p 439-798
4. J.O. Peters and G. Lutjering, Comparison of Fatigue Fracture of $\alpha+\beta$ and β Titanium Alloys, *Metal. Mater. Trans. A,* Vol 32, 2001, p 2805-2818
5. S. Muneki, F. Morito, J, Takahashi, T. Kainuma, and Y. Kawabe, High Cycle Fatigue Properties of Beta Titanium Alloys, *Metallurgy and Technology of Practical Titanium Alloys,* 1st ed., S. Fujishiro, D. Eylon, and T. Kishi, Ed., The Materials Society, 1994, p 191-197
6. R.R. Boyer, W.J. Porter, E.R. Barta, and D. Eylon, Microstructure/ Properties Relationships inTi-15V-3Cr-3Al-3Sn High Strength Castings, *Microstructure/ Property Relationships in Titanium Aluminides and Alloys,* 1st ed., Y.W. Kim and R.R. Boyer, Ed., The Materials Society, 1991, p 511-520
7. J.G. Ferrero, J.R. Wood, and P.A. Russo, Microstructural/Mechanical Property Relationships in Bar Products of Beta-C (Ti-3Al-8V-6Cr-4Mo-4Zr), *Beta Titanium Alloys of the 1990s,* 1st ed., D. Eylon, R.R. Boyer, and D.A. Koss, Ed., The Materials Society, 1993, p 211-226
8. R.R. Boyer, H.J. Rack, and V. Venkatesh, The Influence of Thermomechanical Processing on the Smooth Fatigue Properties of Ti-15V-3Cr-3Al-3Sn, *Mater. Sci. Eng. A,* Vol 243, 1998, p 97-102
9. L. Wagner and J.K. Gregory, Improvement of Mechanical Behavior in Ti-3Al-8V-6Cr-4Mo-4Zr by Dupex Aging, *Beta Titanium Alloys of the 1990s,* 1st ed., D. Eylon, R.R. Boyer, and D.A. Koss, Ed., The Materials Society, 1993, p 199-210
10. W.N. Stroh, The Formation of Cracks as a Result of Plastic Flow, *Proc. R. Soc. London, Ser. A,* Vol 223, 1954, p 404-414
11. J. Gurland, The Measurement of Grain Contiguity in Two-Phase Alloys, *Trans. AIME,* Vol 212, 1958, p 452-455